Journal of ELECTRONIC MATERIALS, Vol. 44, No. 8, 2015
DOI: 10.1007/s11664-015-3688-6
© 2015 The Minerals, Metals & Materials Society

Investigation of the Magnetic and Optical Properties of Wurtzite Fe-Doped ZnS Nanorods

SUNIL KUMAR[1,2,3] and N.K. VERMA[1]

1.—Nano Research Lab, School of Physics and Material Science, Thapar University, Patiala 147 004, Punjab, India. 2.—Department of Physics, Indus International University, Una 174301, Himachal Pradesh, India. 3.—e-mail: skt.nano@gmail.com

The optical and magnetic properties of Fe-doped ZnS nanorods have been investigated at room temperature. X-ray diffraction revealed the doped and undoped nanorods had a wurtzite crystal structure. The lattice constants of Fe-doped ZnS nanorods were less than those of the undoped counterpart. The elemental composition of the Fe-doped ZnS nanorods was verified by use of electron dispersive spectroscopy, which confirmed the presence of Fe. Compared with the undoped counterpart, a blue shift in the absorption edge was observed for Fe-doped ZnS nanorods. Blue and green emission lines were obtained from undoped and Fe-doped ZnS nanorods at 447 nm and 533 nm, respectively. Study of photoluminescence intensity revealed quenching at higher Fe concentration. The ferromagnetic character induced in Fe-doped ZnS nanorods was analyzed by use of M–H curves. Magnetic saturation initially increased with increased Fe doping up to 5%, then decreased with Fe doping up to 10%.

Key words: Nanorods, dilute magnetic semiconductors, blue-shift, quenching, ferromagnetism

INTRODUCTION

There has recently been much interest in research on transition metal-doped chalcogenide nanomaterials, materials more popularly known as dilute magnetic semiconductors (DMS).[1] Because of their charge and spin-controlling features, DMS materials have attracted much interest in the scientific community. These materials have found applications in spintronics, band-gap engineering devices, light emitting diodes, field detectors, lasers, magnetic resonance imaging (MRI), and solar cells.[2–7] II–VI compounds, for example CdS, CdSe, ZnS, ZnO, and ZnSe are popular host materials which are doped with transition metals or rare-earth metals.[8–13] ZnS, a wide-band-gap material (3.6 eV), has fascinated researchers because of its wide range of applications. Addition of 3d transition metals to ZnS at the nanoscale is important because nanorods have unique properties as a result of quantum confinement effects and shape anisotropy. These nanorods have applications as interconnects in a variety of nanoelectromechanical systems (NEMS) which are difficult to achieve with their bulk counterparts. Since the discovery of Mn-doped ZnS nanocrystals by Bhargawa et al. in 1994,[14] attempts have been made by the scientific community to investigate the optical and magnetic properties of ZnS-based DMS nanostructures. Bhattacharya et al. studied the electrical and magnetic properties of cold compacted Fe-doped ZnS nanoparticles. In another study on Fe-doped ZnS nanomaterials, a continuous increase of magnetization was observed at low temperature.[15] Sambavisham et al. reported the magnetism induced in Fe-doped ZnS nanoparticles.[16] It was found that undoped ZnS has diamagnetic behavior whereas Fe-doped ZnS nanomaterials have superparamagnetic-like behavior indicative of weak ferromagnetism. Eryong et al. observed reductions in the photoluminescence (PL) intensity and superparamagnetism of Fe-doped ZnS nanoparticles.[17]

(Received July 2, 2014; accepted February 5, 2015; published online February 27, 2015)

Although several other studies of the PL and magnetic properties of transition metal-doped ZnS nanostructures have also been reported in the literature,[18–26] room-temperature magnetism induced in transition metal-doped ZnS DMS nanostructures remains a challenge.

In the work discussed in this report, the structural, optical, and magnetic properties of Fe-doped nanorods, synthesized by use of a low-temperature solvothermal technique, were studied. Few reports of magnetic studies of Fe-doped ZnS nanorods revealing a ferromagnetic behavior at room temperature are available in the literature.

EXPERIMENTAL

Synthesis

All reagents and solvents were of analytical grade and were used without further purification. Zinc acetate was used as a source of Zn, thiourea as a source of sulfur, iron chloride as a source of Fe, and a mixture of water and ethylenediamine (en) as solvent (1:1). ZnS nanorods were synthesized by use of a solvothermal technique described in the literature,[18] with few modifications. In a typical procedure, zinc acetate and thiourea at the required concentrations were dissolved in 70 ml of the en–water mixture. For Fe doping, the required concentration of iron chloride was added to the mixture. This solution was placed in a 100-ml Teflon-lined stainless-steel chamber which was then sealed and placed in a hot air oven at 180°C for 10 h. The resulting white solution was left to cool at room temperature then washed many times with water and acetone. The white powder obtained was dried for 6 h at 80°C.

Characterization

Morphology was studied by transmission electron microscopy (TEM) and high-resolution transmission electron microscopy (HRTEM), by use of an FEI Technai F30 electron microscope. X-ray diffraction (XRD) studies were conducted with a PANalytical X'Pert Pro XRD instrument, using the characteristic wavelength of copper, λ = 1.54 Å. Optical properties were studied by use of a fluorescence spectrophotometer (LS55, Perkin Elmer) and a UV–visible (UV–Vis) spectrophotometer (Specord-205, Analytik Jena). Elemental analysis was performed with Oxford Analytical equipment coupled with a scanning electron microscope (SEM). Magnetic studies were performed by use of a vibrating sample magnetometer (VSM, Lake Shore 7040).

RESULTS AND DISCUSSION

Morphological and Elemental Analysis

The morphology of undoped and Fe-doped ZnS nanorods was studied by use of TEM and HRTEM images (Fig. 1a and b). It is clear that Fe-doped ZnS nanorods are morphologically identical with the

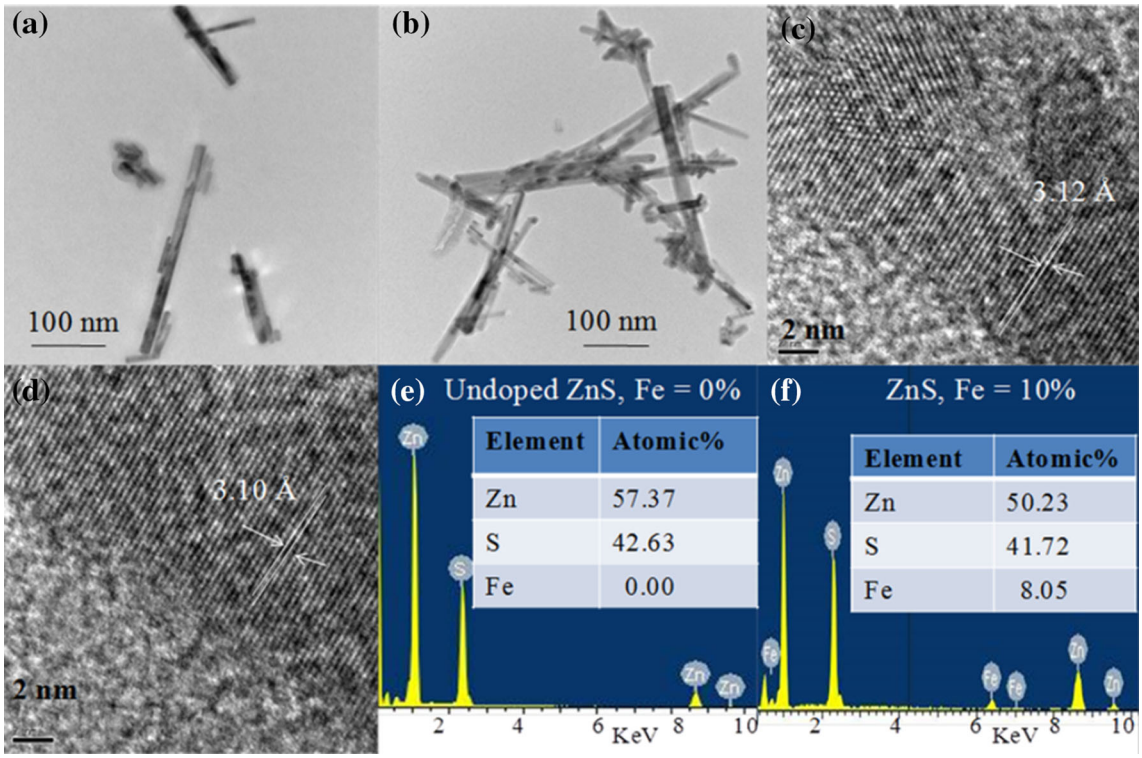

Fig. 1. TEM images of (a) undoped and (b) 10% Fe:ZnS; HRTEM images of (c) undoped and (d) 10% Fe:ZnS; EDS spectra of (e) undoped and (f) 10% Fe:ZnS nanorods.

undoped counterparts. The average diameter of the nanorods was ~10 nm and the length varied between 50 and 400 nm. HRTEM images (Fig. 1c and d) revealed the atomic spacing was 3.12 Å for undoped ZnS nanorods, which accords well with the d-spacing of the (002) plane in XRD spectra of standard ZnS. The corresponding atomic spacing of 10% Fe-doped ZnS nanorods was 3.10 Å, slightly less than for the undoped counterpart. Elemental analysis of undoped ZnS and 10% Fe-doped ZnS nanorods was performed on the basis of EDS spectra (Fig. 1e and f) . The presence of Fe is clearly indicated in the spectrum obtained from the doped nanorods, although the observed amount of Fe is lower than the actual amount doped. This may be because of loss of Fe during extensive washing of the ZnS samples.

STRUCTURAL STUDIES

The structural properties were analyzed by use of XRD patterns. The XRD patterns of undoped and Fe-doped nanorods are shown in Fig. 2.

Diffraction peaks were observed at $2\theta = 26.5°$, 28.8°, 30.5°, 39.8°, 47.6°, 51.8° and 56.5° corresponding to, respectively, the (100), (002), (101), (102), (110), (103), and (112) peaks. These peaks can be indexed to the wurtzite phase (JCPDS card no. 36-1450). No extra peaks of secondary phases were observed for Fe-doped samples, which indicates that Fe has been substituted in the ZnS lattice. The preferred orientation of a particular crystal plane was determined by determination of the texture coefficient, TC(*hkl*), by use of the relationship[19]:

$$\mathrm{TC}(hkl) = \frac{I(hkl)}{I'(hkl)}\left[\frac{1}{n}\frac{I(hkl)}{I'(hkl)}\right]^{-1} \quad (1)$$

where *I'(hkl)* is intensity of standard JCPDS peaks, *I(hkl)* is the intensity of the corresponding peaks observed experimentally, and *n* is the number of peaks in the XRD patterns. It was observed that the TC(002) value was largest, indicating the (002) plane was the preferred direction of growth. The corresponding lattice constants calculated along the (002) plane are listed in Table I.

Clearly, there is a slight shift in the peak position toward higher diffraction angle with increased Fe concentration; this may be ascribed to smaller ionic radius of Fe^{2+} compared with Zn^{2+}. It was observed that as the Fe concentration was increased, the lattice constants decreased slightly, which indicates that the Fe-doped ZnS structure is under compressive strain because of the smaller radii of the Fe ions compared with the Zn ions. The *d*-spacing values decreased with increasing Fe concentration. These results accord well with HRTEM observations.

Optical Studies

UV–Vis Studies

Absorption spectra of undoped and Fe-doped ZnS nanorods, recorded in the range 250–400 nm, are

Table I. Lattice constants along (002) plane for undoped and Fe-doped ZnS nanorods

Fe concentration (%)	λ_{max} (nm)	Band gap (eV)
0.0	270	4.59
1.0	267	4.64
5.0	265	4.67
10.0	260	4.78

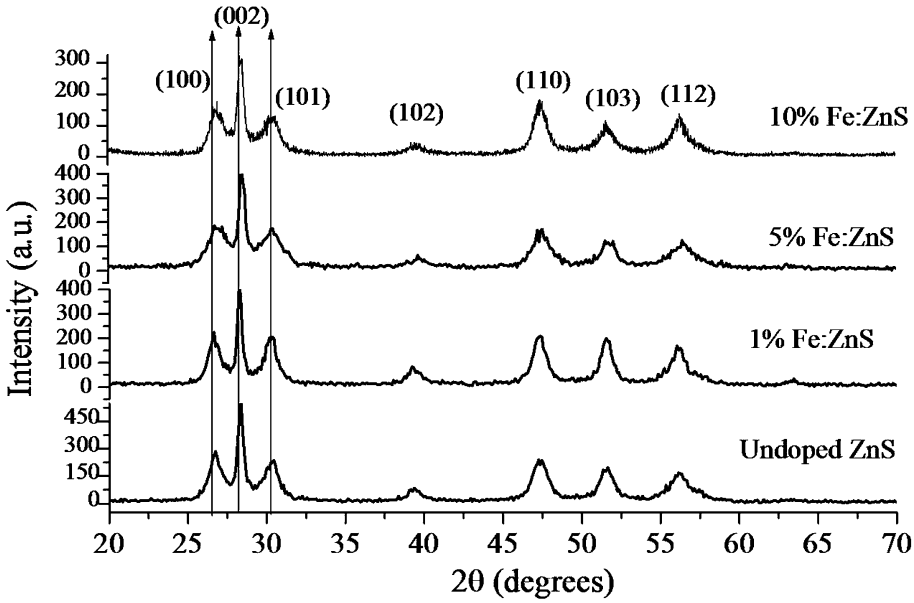

Fig. 2. XRD patterns of undoped and Fe-doped nanorods.

shown in Fig. 3. It is clear that the wavelengths of maximum absorbance (λ_{max}) occur at 270, 267, 265, and 260 nm, respectively, for undoped nanorods and nanorods containing 1%, 5%, and 10% Fe; this is indicative of a blue shift compared with the bulk and undoped counterparts. The blue shift compared with bulk ZnS may be ascribed to quantum confinement effects,[20] and the blue shift in the absorption edge of Fe-doped ZnS nanorods may be because the radius of Fe ions is smaller than that of the replaced Zn ions in the ZnS lattice. Similar observations have been reported in the literature for Fe-doped ZnS nanoparticles and thin films.[16,21] The effect of Fe concentration on the blue shift of the absorption edge is summarized in Table II. In the literature, the blue shift of the band gap as a result of external doping has also been attributed to new energy levels arising in the ZnS energy band as a result of the presence of the dopant.[22]

PL Studies

PL emission spectra obtained at an excitation wavelength, λ_{ex}, of 300 nm are shown in Fig. 4. The two broad peaks at 447 nm and 533 nm are indicative of blue and green emission, respectively. The blue emission at 447 nm may be attributed to radiative recombination of sulfur vacancies related to donor energy levels and the purity of the ZnS host material. The PL intensity increases with increasing Fe concentration up to 5%. As the Fe concentration is increased further, up to 10%, quenching of the PL occurs. The greater PL intensity at lower doping concentrations may be because at lower Fe concentrations the possibility of trapping Fe ions inside the ZnS matrix is increased, which may result in vacancies at interstitial sites or at lattice positions. This may create new radiation centers, resulting in increased intensity.[23] As the Fe concentration is increased further up to 10%, the doped Fe ions interfere with the radiative recombination which hides the effect of creation of new radiation centers, resulting in quenching of the fluorescence intensity. Similar observations for Ni-doped ZnS nanorods have been reported in the literature.[10,24]

Magnetic Studies

M–H curves obtained at room temperature (300 K) up to 2 T are shown in Fig. 5. The curves indicate that undoped ZnS nanorods have diamagnetic character whereas the Fe-doped ZnS nanorods have ferromagnetic character (Fig. 5a). As the magnetic field is increased to 2 T a sharp decrease in magnetization occurs, as is clear from Fig. 5b. The M–H curves are indicative of remanent magnetization of 0.00034, 0.0013, 0.002, and 0.0016 emu/g for undoped ZnS nanorods and 1%, 5% and 10% Fe-doped ZnS nanorods, respectively, with corresponding saturation magnetization of 0.0065, 0.01, and 0.0095 emu/g, respectively, for the doped nanorods (Fig. 5c). The low coercivity of all the samples is indicative of soft magnetic behavior. It is clear that the saturation magnetization persists up to 5000 Oe for all samples. As the magnetic field is

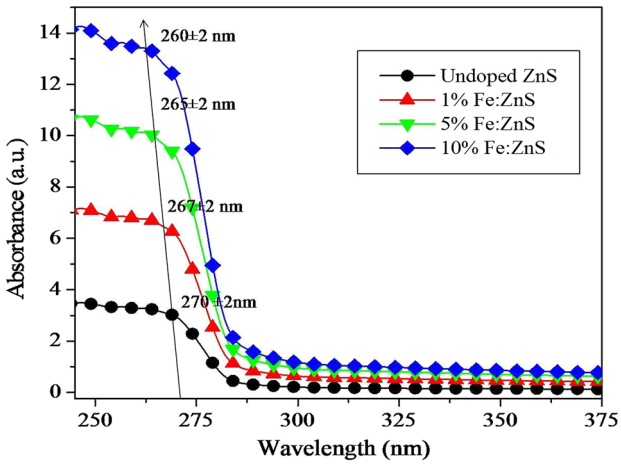

Fig. 3. UV-Vis spectra of undoped and Fe-doped nanorods.

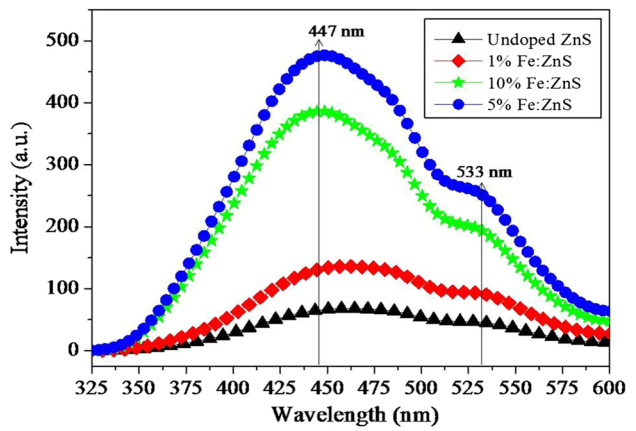

Fig. 4. PL spectra of undoped and Fe-doped nanorods.

Table II. Variation of the band gap with Fe concentration

Sample	Peak position	*d*-spacing (Å)	Lattice constants
Undoped ZnS	28.32	3.138 ± 0.005	a = 3.836, c = 6.297
1% Fe:Zns	28.37	3.133 ± 0.005	a = 3.830, c = 6.287
5% Fe:Zns	28.43	3.128 ± 0.005	a = 3.823, c = 6.272
10% Fe:Zns	28.59	3.124 ± 0.005	a = 3.817, c = 6.238

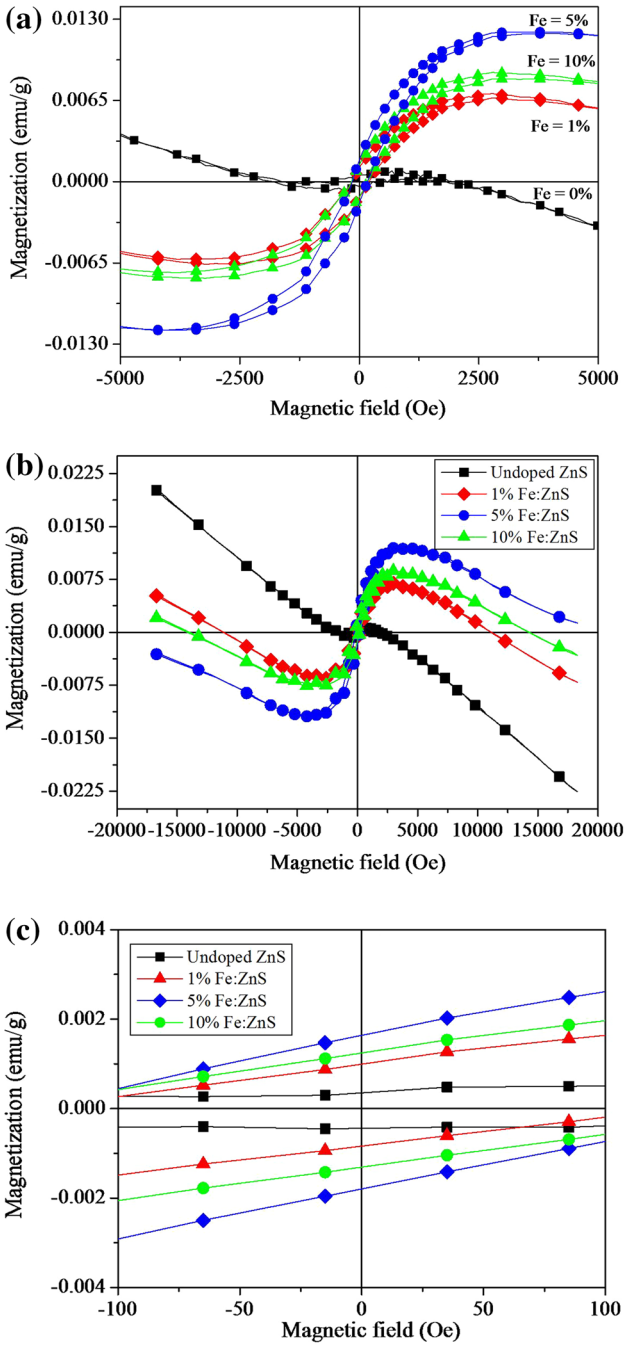

Fig. 5. M–H curves of undoped and Fe-doped nanorods indicating (a) ferromagnetic behavior; (b) complete view of M–H curves up to 2 T and (c) magnified view of M–H curves.

increased further to 1.5 T, there is a sharp decrease in the magnetization. This behavior clearly indicates that insertion of Fe ions in the ZnS matrix induces ferromagnetic character in the doped ZnS nanorods. The ferromagnetic behavior could be because of aggregation of Fe atoms in the ZnS lattice, but this possibility can be disregarded, because no secondary phases were observed in XRD spectra. Fe-doped ZnS nanorods have ferromagnetic character which increases with increasing Fe concentration up to 5%, but as the concentration is increased further to 10% the saturation magnetization is reduced. The ferromagnetism at lower concentrations may be ascribed to intrinsic coupling between doped Fe–Fe atoms.[25] As the concentration is further increased to 10% the Fe–Fe distance is reduced which may cause antiferromagnetic interaction which, in turn, causes a decrease in the magnetization. Similar observations for Ni-doped and Co-doped ZnS nanoparticles have been reported in the literature.[24,26] It has been stated that reduced magnetization arises because of competition between antiferromagnetic and ferromagnetic ordering.

CONCLUSIONS

Undoped and Fe-doped ZnS cylindrical nanorods with the wurtzite crystal structure were synthesized by use of a low-temperature solvothermal technique. The nanorods were of average diameter ~10 nm and length 50–400 nm. The absence of any impurity in the XRD spectra confirmed doping of the ZnS lattice with Fe ions. The reduction in lattice constants also supports doping of the ZnS lattice with Fe. The blue-shift of the band gap with increasing Fe concentration may be attributed to the small size of Fe compared with Zn and the creation of new energy levels. PL intensity increased with increasing Fe ion concentration up to 5%; at 10% Fe doping, however, the intensity was quenched. M–H curve analysis revealed the ferromagnetic character of Fe-doped ZnS nanorods. The saturation magnetization increased up to 5% Fe concentration, because of intrinsic coupling, whereas at 10% Fe concentration it decreased, because of antiferromagnetic interactions. The low coercivity of Fe-doped ZnS nanorods is indicative of soft magnetic behavior.

REFERENCES

1. H. Ohno, *Science* 281, 951 (1998).
2. J.K. Furdyna, *J. Appl. Phys.* 64, R29 (1988).
3. M.L. Steigerwald and L.E. Brus, *Acc. Chem. Res.* 23, 183 (1990).
4. D. Kim, K.D. Min, J. Lee, J.H. Park, and J.H. Chun, *Mater. Sci. Eng. B* 131, 13 (2006).
5. Y. Wang and N. Herron, *J. Phys. Chem.* 95, 525 (1991).
6. V.L. Colvin, M.C. Schlamp, and A.P. Alivisatos, *Nature* 370, 354 (1994).
7. R.N. Bharagava, *J. Lumin.* 70, 85 (1996).
8. C.C. Chen, Y.J. Hsu, Y.F. Lin, and S.Y. Lu, *J. Phys. Chem. C* 112, 17964 (2008).
9. S. Kumar, S. Kumar, N.K. Verma, and S.K. Chakravarti, *J. Mater. Sci.* 22, 1456 (2011).
10. Z. Jindal and N.K. Verma, *Mater. Chem. Phys.* 124, 270 (2010).
11. K. Kaur, G.S. Lotey, and N.K. Verma, *Mater. Chem. Phys.* 143, 141 (2013).
12. G.S. Lotey, J. Singh, and N.K. Verma, *J. Mater. Sci.* 24, 3611 (2013).
13. G.S. Lotey, Z. Jindal, V. Singhi, and N.K. Verma, *Mater. Sci. Semicond. Process.* 16, 2044 (2013).
14. R. Bhargava, D. Gallagher, and T. Welker, *J. Lumin.* 60, 275 (1994).

15. S. Bhattacharya and D. Chakravorty, *Chem. Phys. Lett.* 444, 319 (2007).
16. S. Sambasivam, D.P. Joseph, J.G. Lin, and C. Venkateswaran, *Mater. Sci. Eng. B* 150, 125 (2008).
17. N. Eryong, L. Donglai, Z. Yunsen, B. Xue, Y. Liang, J. Yong, J. Zhifeng, and S. Xiaosong, *Appl. Surf. Sci.* 257, 8762 (2011).
18. S. Biswas and S. Kar, *Nanotechnology* 19, 045710 (2008).
19. Z. Yang, Q.H. Liu, H.C. Yu, B. Zou, Y.G. Wang, and T.H. Wang, *Nanotechnology* 19, 035704 (2008).
20. L. Zhang, D. Qin, G. Yang, and Q. Zhang, *Chalcogenide Lett.* 9, 93 (2012).
21. J. Cao, D. Han, B. Wang, L. Fan, H. Fu, M. Wei, B. Feng, X. Liu, and J. Yang, *J. Solid State Chem.* 200, 317 (2013).
22. K.T. Al-Rasoul, N.K. Abbas, and Z.J. Shanan, *Int. J. Electrochem. Sci.* 8, 5594 (2013).
23. N. Dixit, N. Anasane, M. Chavda, D. Bodas, and H.P. Soni, *Mater. Res. Bull.* 48, 2259 (2013).
24. S. Kumar and N.K. Verma, *J. Mater. Sci.* 25, 785 (2014).
25. M.A. Shafique, S.A. Shah, M. Nafees, K. Rasheed, and R. Ahmad, *Int. Nano Lett.* 2, 31 (2012).
26. S. Sambasivama, D. Paul Joseph, J.G. Lin, and C. Venkateswaran, *J. Solid State Chem.* 182, 2598 (2009).